Available online at www.sciencedirect.com
ScienceDirect
Biochimica et Biophysica Acta 1768 (2007) 728–736
Biochimica et Biophysica Acta
BBA
www.elsevier.com/locate/bbamem

Effects of freezing on membranes and proteins in LNCaP prostate tumor cells

Willem F. Wolkers [a,*], Saravana K. Balasubramanian [a], Emily L. Ongstad [d], Helena C. Zec [e], John C. Bischof [a,b,c]

[a] Department of Mechanical Engineering, University of Minnesota, Minneapolis, MN 55455, USA
[b] Department of Biomedical Engineering, University of Minnesota, Minneapolis, MN 55455, USA
[c] Department of Urologic Surgery, University of Minnesota, Minneapolis, MN 55455, USA
[d] Department of Biomedical Engineering, Michigan Technological University, Houghton, MI 49931-1295, USA
[e] Department of Biomedical Engineering, Worcester Polytechnic Institute, Worcester, MA 01609-2280, USA

Received 11 October 2006; received in revised form 7 December 2006; accepted 11 December 2006
Available online 13 December 2006

Abstract

Fourier transform infrared spectroscopy (FTIR) and cryomicroscopy were used to define the process of cellular injury during freezing in LNCaP prostate tumor cells, at the molecular level. Cell pellets were monitored during cooling at 2 °C/min while the ice nucleation temperature was varied between −3 and −10 °C. We show that the cells tend to dehydrate precipitously after nucleation unless intracellular ice formation occurs. The predicted incidence of intracellular ice formation rapidly increases at ice nucleation temperatures below −4 °C and cell survival exhibits an optimum at a nucleation temperature of −6 °C. The ice nucleation temperature was found to have a great effect on the membrane phase behavior of the cells. The onset of the liquid crystalline to gel phase transition coincided with the ice nucleation temperature. In addition, nucleation at −3 °C resulted in a much more co-operative phase transition and a concomitantly lower residual conformational disorder of the membranes in the frozen state compared to samples that nucleated at −10 °C. These observations were explained by the effect of the nucleation temperature on the extent of cellular dehydration and intracellular ice formation. Amide-III band analysis revealed that proteins are relatively stable during freezing and that heat-induced protein denaturation coincides with an abrupt decrease in α-helical structures and a concomitant increase in β-sheet structures starting at an onset temperature of approximately 48 °C.

Keywords: Cryosurgery; Cryopreservation; FTIR; Membrane phase behavior; Prostate tumor cell; Protein denaturation

1. Introduction

Cryosurgery is becoming an established therapy for prostate cancer [1,2]. The general mechanisms of injury during cryosurgery typically include direct injury to the cancer cells due to the freezing event, as well as host-mediated events such as vascular injury and immunological effects, which occur after thawing.

One of the factors that determine the type of damage during freezing is the cooling rate [3]. At fast cooling rates, intracellular ice formation is primarily responsible for the destruction of cells. By contrast, at slow cooling rates, where dehydration predominates, osmotic injury due to solute effects causes damage. During slow cooling, ice forms outside the cell before propagating inside the cell [4]. As soon as ice forms outside of a cell in solution, the cell dehydrates, and endogenous biomolecules are exposed to high concentrations of solutes [5]. Rapid freezing, on the other hand, results in lethal intracellular ice formation. The mechanism by which intracellular ice damages cells is not entirely clear, but it has been suggested that cells do not die during the freezing event itself, but during thawing [4]. One other important determinant of intracellular ice formation is the nucleation temperature of ice formation in the extracellular space [6]. Kinetic model studies have shown that the lower the nucleation temperature, the greater is the incidence of intracellular ice formation [7,8].

Abbreviations: FTIR, Fourier transform infrared spectroscopy; IIF, intracellular ice formation; Tm, membrane phase transition temperature

* Corresponding author. Tel.: +1 612 625 4461; fax: +1 612 625 4344.
E-mail address: wolkers@umn.edu (W.F. Wolkers).

0005-2736/$ - see front matter © 2007 Elsevier B.V. All rights reserved.
doi:10.1016/j.bbamem.2006.12.007

At the molecular level, freezing affects membrane lipids, proteins and nucleic acids by changing the hydrophobic and hydrophilic interactions determining structure and function. It is well established that cooling alters the physical state of lipids, thus altering lipid organization and fluidity [9]. Biological membranes often exhibit a liquid crystalline to gel phase transition during cooling and vice versa during re-warming [10]. The consequences of such phase transitions are thought to include increased membrane permeability and lateral phase separation of membrane components. Intracellular proteins may undergo irreversible structural alterations with freezing, due to exposure to high solute concentration [5]. In addition, proteins and lipids are exposed to reactive oxygen species, because enzymatic scavenging systems are compromised by freezing. Reactive oxygen species result in lipid peroxidation and phospholipid de-esterification [11]. In a previous study, we have shown that freezing of AT-1 Dunning tumor cells results in accumulation of free fatty acids [12]. The changed physical properties and chemical composition of the plasma membrane may lead to leakage of cytoplasmic solutes. Proteins are also subject to free radical attack by reactive oxygen species [13]. Moreover, proteins may also be degraded by proteases originating from lysosomes that lost membrane integrity during freezing or thawing [12].

One of the few suitable techniques to study freezing-induced changes in structure and conformation of cellular biomolecules is Fourier transform infrared spectroscopy (FTIR). The CH_2 stretching vibration of lipids, for example, has been used to detect phase transitions in lipids, isolated biological membranes and in whole cells [10,14]. The amide-I, -II, and -III bands, arising from vibrations of the protein backbone, have been widely used to determine the secondary structure of isolated proteins [15–17], and are diagnostic for the overall protein secondary structure of cells and tissues [18]. Most FTIR studies rely on the amide-I band for protein secondary structure analysis. Recent studies, however, have implicated the amide-III band for FTIR protein analysis, because the different types of secondary structure are better resolved, and because this region of the spectrum does not find interference from water and water vapor bands [19,20].

In this work, FTIR was used to study changes in membrane lipid phase behavior and overall protein secondary structure during freezing of LNCaP prostate tumor cells. Samples were nucleated at temperatures ranging from −3 °C to −10 °C. We show that the temperature at which ice is formed in the system affects the membrane phase behavior of the cells. This is explained in terms of cellular dehydration and intracellular ice formation, which both critically depend on the nucleation temperature. Proteins were found to be relatively stable during freezing.

2. Materials and methods

2.1. Cell culture techniques

LNCaP cells were grown in DMEM F-12 media (Gibco, Grand Island, NY, USA) supplemented with 5% fetal bovine serum (FBS), 1% penicillin/streptomycin in saline (Invitrogen, Gaithersburg MD, USA), 250 nM dexamethasone (Sigma-Aldrich, St. Louis, MO, USA) and 5% CO_2 at 37 °C. Cells were grown in 250 ml *T* flasks, harvested by treatment with 0.5 ml Trypsin-EDTA (0.05% Trypsin, and 0.53 mM EDTA (Gibco, Gaithersburg, MD, USA)) for 3 min at 37 °C. About 10 ml of DMEM F-12 medium was added to neutralize the trypsin. The cells were then centrifuged at 1000×*g* for 10 min, the medium was removed, and the cell pellet spread between two CaF_2 IR windows for subsequent FTIR analysis.

2.2. FTIR studies

Infrared absorption measurements were carried out with a Nicolet Magna 750 Fourier transform infrared spectrometer (Thermo-Nicolet, Madison, WI, USA), equipped with a TGS detector. The optical bench was continuously purged with dry air (Balston, Haverhill, MA, USA). The acquisition parameters were: 4 cm^{-1} resolution, 32 co-added interferograms, 4000–900 cm^{-1} wavenumber range. Spectral analysis and display were carried out using Omnic software (Thermo-Nicolet, Madison, WI, USA). About 10 µl of cell pellet was sandwiched between two CaF2 windows separated by a 6 µm mylar spacer (Thermo Electron North America Inc., Madison, WI, USA). Samples were then mounted into a home-made variable temperature cell. Liquid nitrogen was used as a coolant, and the temperature was regulated by a temperature controller (Minco Products Inc., Minneapolis, MN, USA). The temperature of the sample was recorded separately using a thermocouple that was located close to the sample. The temperature dependence of the FTIR spectra was studied by cooling the sample from ambient temperature down to temperatures as low as −80 °C at a rate of approximately 2.0 °C min^{-1}. Cell pellet samples that were cooled at a rate of −2 °C min^{-1} showed ice formation at around −10 °C. The nucleation temperature was increased using *Pseudomonas syringae* (ATCC, Rockville, MD, USA) as a natural ice nucleator according to Devireddy et al. [21]. Five µl of *P. syringae* (10 mg/ml) was placed at the edge of the cell pellet on the IR window. This resulted in nucleation temperatures ranging from −4 to −8 °C. Controlled nucleation at −3 °C and −6 °C was achieved by inserting a copper wire cooled with liquid nitrogen directly into the sample. The heating phase of the experiment was started after a hold time of 5 min. Spectra were recorded over a temperature range from −80 °C to +90 °C at a heating rate of 2 °C min^{-1}.

Membrane fluidity was monitored by observing the position of the CH_2 symmetric stretching band at approximately 2850 cm^{-1}, as described previously [22]. Wavenumber (νCH_2) versus temperature plots were constructed, and phase transition temperatures were determined from the maxima in the first derivatives of the νCH_2 versus temperature plots. The slope at the phase transition temperature, Tm, was taken as a measure for the co-operativity of the phase transition [22]. Phase changes of water into ice and vice versa were determined by plotting the area of the water band between 2680 and 1950 cm^{-1} (H_2O bending and libration combination band) as a function of temperature. Protein denaturation was determined as previously described [12,23]. Briefly, the spectral region between 1700 and 1500 cm^{-1} containing the amide-I and -II absorption bands was selected. Heat denaturation profiles were obtained by subtracting spectra recorded at 20 °C from spectra at the indicated temperatures. The second derivatives of these difference spectra were taken with a 13-point smoothing factor to resolve the different bands more clearly. Thermal denaturation of proteins was followed by monitoring the area of bands at 1625 cm^{-1} (amide-I region) and 1550 cm^{-1} (amide-II region) that become visible upon heating of the sample. The areas of these bands were plotted as a function of temperature, and used to determine the onset and midpoint of protein denaturation. The amide-III region, located between 1350 and 1200 cm^{-1}, was also analyzed to corroborate the amide-I and II band analysis. In this case, the area under the original absorbance spectra was calculated and plotted as a function of temperature. Bands at approximately 1315 and 1235 cm^{-1} were found to decrease and increase, respectively, upon protein denaturation.

2.3. Prediction of cellular biophysics: intracellular ice formation and dehydration

Previously described biophysical models [24–26] were used to predict the cellular biophysics in LNCaP cells during freezing, including cellular

dehydration and intracellular ice formation (IIF). The model is described in detail elsewhere [26] and requires cell-specific water transport and intracellular ice formation parameters to be determined through experimentation. Briefly, cellular dehydration and intracellular ice formation are dependent on a variety of freezing and cell-specific parameters as shown in Eqs. (1) and (2), respectively.

$$\frac{dV}{dT} = f\left(L_{pg}, E_{Lp}, A, V_o V_b, B\right) \quad (1)$$

In the above equation for water transport, T is the temperature (°K), L_{pg} is the cell membrane hydraulic permeability at a reference temperature of 273.15 °K (μm/min atm), E_{Lp} is the activation energy for water transport (kcal/mol), V_o is the isotonic cell volume (μm^3), V_b is the bound water volume (μm^3), and B is the cooling rate. The equation below describes the probability of intracellular ice formation:

$$\mathrm{PIF} = f(\Omega_o, \kappa_o, A, T, \Delta T, B) \quad (2)$$

Here, additional parameters include: Ω is the kinetic nucleation parameter for heterogeneous ice nucleation (1/m^2 s), κ is the thermodynamic nucleation parameter (°K^5) and ΔT is the degree of undercooling of the cytoplasm (°K). The parameters that were used as input for this model were obtained by fitting the biophysical behavior of LNCaP cells as previously reported for numerous cell types [27–29]. Specific water transport parameters for LNCaP cells were found by fitting Eq. (1) to the dehydration behavior of $n=10$ to 30 cells at 5, 10 and 25 °C/min, where no intracellular ice formation occurred. Similarly, Eq. (2) was used to fit the intracellular ice formation behavior of $n=50$ to 75 cells at 130 °C/min, a rate where cellular dehydration was minimal. The model was fit to the data using a Marquardt optimization scheme, as previously described [27,28]. Once obtained, the biophysical parameters were used along with Eqs. (1) and (2) to predict the biophysical response of the cells under the freezing conditions used in this study which include cooling at 2 °C/min and nucleation at different subzero temperatures.

2.4. Viability

For viability measurements, cell pellets were frozen between glass microslides using a Linkam Scientific conduction type cryostage (Linkam, Tadworth, UK). Samples were cooled at a rate of 2 °C min^{-1}, and nucleated at the indicated temperatures using a liquid nitrogen-cooled copper wire. The end temperature was −20 °C, and after a hold time of 5 min, the sample was re-warmed at a rate of 2 °C min^{-1} to room temperature. After thawing, the slides were separated, dyes were loaded onto the cellular film, and the slides were covered with glass cover slips before microscopic evaluation. Both frozen and control samples were loaded, by a 30 min incubation at 37 °C, with Hoechst 33258 (Sigma, St. Louis, MO, USA) which stains the DNA of all the cells, and Propidium Iodide (Molecular Probes, Eugene, OR, USA), which stains the DNA only of cells with disrupted membranes, as previously described [12]. The numbers of live and dead cells were counted using a BX-50 Olympus fluorescence microscope (Leeds Precision, Minneapolis, MN, USA). Three to five fields with 30–40 cells per field were counted for each sample. Based on the number of live cells obtained from the assay, viability is represented in terms of percent viability.

3. Results

3.1. Cell biophysics and viability

Based on experimental freezing results fit to Eqs. (1) and (2), the biophysical parameters of LNCaP cells were obtained (Table 1) and the model was used to predict intracellular ice formation and cellular dehydration during freezing conditions relevant to the FTIR studies. The parameters depicted in Table 1 were used to construct Fig. 1, which shows the effect of the nucleation temperature versus the predicted incidence of intracellular ice formation (Fig. 1A) and cellular dehydration (Fig. 1B). These predictions show that intracellular ice formation is avoided when nucleation is achieved between 0 and −4 °C. At nucleation temperatures below −4 °C, the percentage of intracellular ice formation increases, and at nucleation temperatures below −6 °C, the incidence of intracellular ice formation is 100%. Any dehydration that occurs after nucleation will reduce the total amount of lethal intracellular ice within the cells. Thus, if LNCaP cell samples are nucleated between 0 and −4 °C a drastic decrease in cell volume with no intracellular ice formation is predicted. If nucleation occurs between −4 and −6 °C, both dehydration and intracellular ice formation occur simultaneously, whereas minimal dehydration and maximal intracellular ice formation is expected below −6 °C.

It should be noted that the temperature at which intracellular ice formation occurs, along with the amount of water within the cell at that point, will determine the total amount of intracellular ice. More than 5–10% normalized intracellular water in the ice phase is considered lethal to most cells, while amounts less than this are often tolerated and can correlate with survival conditions [4]. If the cells dehydrate too severely, this can also result in cell destruction. Thus, an optimal cooling condition between total dehydration and large stable intracellular ice crystals is expected, as found in the viability curve given. Fig. 1A depicts the effect of the nucleation temperature on survival of cells that were frozen to an end temperature of −20 °C. Cells exhibit optimum survival at a nucleation temperature of −6 °C. This is close to the midpoint of the predicted curve for intracellular ice formation (50% IIF at −5 °C).

3.2. FTIR spectra of LNCaP cells

Fig. 2 depicts IR absorbance spectra of LNCaP cells at 20 °C, +80 °C, and −80 °C. Overall, the IR spectrum of the cells in media is dominated by the signal from water or from ice. Water exhibits strong vibrational bands at around 3300 cm^{-1}, 2200 cm^{-1}, and 1650 cm^{-1} arising from stretching, libration and bending combination, and scissoring vibrational modes, respectively. The frozen sample exhibits clear differences in spectral shape compared to the other samples. This is seen throughout the spectrum and is mostly due to shape changes of the water absorption bands upon transition into ice. In the

Table 1
Parameters used to predict intracellular ice formation and cellular dehydration during freezing of LNCaP cells

Nomenclature	Value	Unit
T=absolute temperature	Variable	°K
B=cooling rate	2	°K/min
V=cell volume	Variable	μm^3
V_o=initial isotonic cell volume	1806	μm^3
V_b=osmotically inactive cell volume	0.07 V_o	μm^3
L_{pg}=reference permeability at 273 K	0.21	μm. (min atm)$^{-1}$
E_{Lp}=apparent activation energy	25.1	kcal/mol
Ω_o=kinetic nucleation parameter	27.7×10^8	(m^2 s)$^{-1}$
κo=thermodynamic nucleation parameter	2.23×10^9	°K^5
PIF=probability of ice formation	Variable	%
ΔT=degree of undercooling of the cytoplasm	Variable	°K

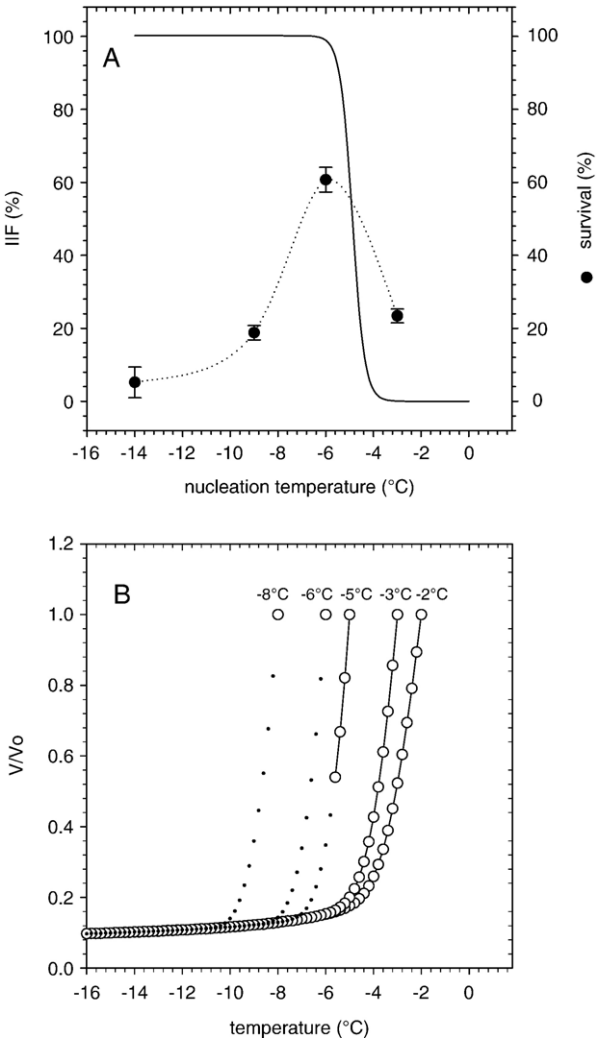

Fig. 1. Biophysical behavior and survival of LNCaP cells after freezing at 2 °C/min and nucleation at various subzero temperatures. (A) Prediction of intracellular ice formation as a function of the ice nucleation temperature (solid line) and the effect of the nucleation temperature on survival (filled circles) of cells that were subsequently frozen down to an end temperature of −20 °C. (B) Decrease in volume of cells versus nucleation temperature. The curves show the decrease in volume upon ice nucleation at subzero temperatures. The solid lines reflect the actual decrease in volume above nucleation of −4 °C, while the dotted lines represent conditions below −4 °C where intracellular ice formation is competing with dehydration to determine the overall cellular response.

3000–2800 cm^{-1} region, the symmetric and asymmetric CH_2 stretching vibrations of lipid acyl chains are visible. Characteristic protein bands are visible at 1655 cm^{-1} (amide-I band) and at 1550 cm^{-1} (amide-II band). The amide-I band overlaps with the scissoring vibrational mode of water. In the amide-III region of the spectrum (1330 and 1200 cm^{-1}), several weak bands are visible.

3.3. Simultaneous FTIR assessment of membrane phase behavior, protein denaturation and ice formation

IR spectra of LNCaP cells as a function of temperature show shifts of bands, associated with gel formation of membrane lipids during cooling (Fig. 3A), formation of ice during cooling (Fig. 3B), and denaturation of proteins during heating (Fig. 3C and D).

Second derivative analysis was used to show the small lipid bands in the 3000–2800 cm^{-1} region more clearly. The symmetric CH_2 stretching mode arising from membrane lipids exhibits a shift to lower wavenumber with decreasing temperature, indicating a decrease in membrane conformational disorder during cooling (Fig. 3A). The band around 2200 cm^{-1}, which arises from a combination of H_2O bending and librational motions, shifts to higher wavenumber upon ice formation and the band width decreases (Fig. 3B).

Fig. 3C shows spectra from cells recorded at various elevated temperatures after subtracting the spectrum taken at 20 °C. Protein denaturation coincides with an abrupt increase in the formation of extended β-sheet structures, as is evident from the increase of the band at around 1625 cm^{-1}. In the amide-II region, denaturation is visible as a sudden decrease of the band at 1550 cm^{-1}. Inspection of the amide-III region shows that a band around 1315 cm^{-1} decreases upon heating, while a band at around 1235 cm^{-1} increases (Fig. 3D). Bands at 1315 cm^{-1} and 1235 cm^{-1} have been assigned to α-helical and β-sheet structures respectively [19].

3.4. Membrane phase behavior is affected by ice formation in the system

The thermotropic response of the symmetric CH_2 stretching vibration shows that the membrane phase behavior of LNCaP cells during cooling is affected by the nucleation temperature (Fig. 4A). When the sample is nucleated at −3 °C, the membranes undergo a highly co-operative phase transition with an onset temperature that coincides with the nucleation temperature of ice in the system. The sample that nucleated at −10 °C exhibited a much less co-operative phase transition with an onset temperature at approximately −10 °C. In addition, the sample that nucleated at −10 °C shows a considerably higher wavenumber at −80 °C, indicating greater residual conformational disorder compared to the sample nucleated at −3 °C. The

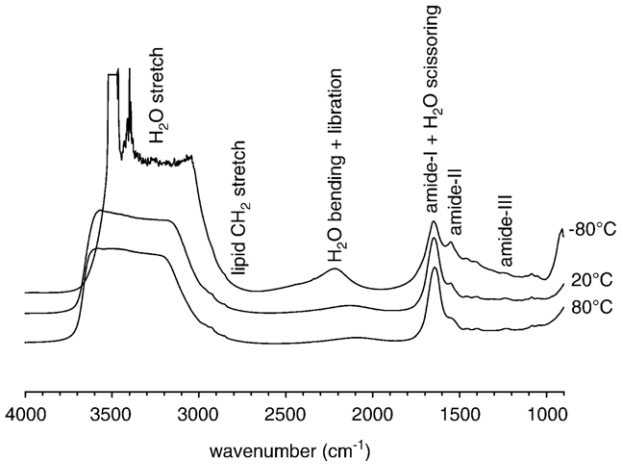

Fig. 2. In situ IR absorption spectra of LNCaP prostate tumor cells at −80, 20, and 80 °C. Characteristic molecular group vibrations are indicated.

sample that was nucleated at −6 °C shows intermediate membrane phase behavior. The co-operativity of the membrane phase transition, expressed as the slope at the midpoint of the transition, showed a correlation with the ice nucleation temperature: the co-operativity decreases with decreasing nucleation temperature (Fig. 5). Taken together, these observations indicate that the onset temperature of the membrane phase transition coincides with the temperature at which ice is formed in the system, and that the nucleation temperature affects the co-operativity of the membrane phase transition and the residual conformational disorder in the frozen state. The highly co-operative phase transition under dehydrating conditions was only observed in intact viable cells (Fig. 4B). Cells that were lysed by pelleting and resuspending in pure water showed a much less co-operative transition and a concomitantly higher wavenumber of the CH_2 stretching vibration in the frozen state.

3.5. Protein stability during freezing and heating

Changes in the amide-I, -II, and -III regions of the spectra upon heating from 20 to 90 °C were used to determine the protein denaturation profile of the cells (see Fig. 3C and D). The formation of extended β-sheet structures upon protein denaturation is evident from the sudden increase in the area of the band at 1625 cm^{-1} in the amide-I region (Fig. 6A). Protein denaturation commences at an onset temperature of 48 °C, and the rate of β-sheet accumulation reaches a maximum at 66 °C (midpoint temperature). Fig. 6B shows that the amide-II band area shows a sudden decrease in area upon denaturation of the sample. This likely reflects a combined effect of a decrease in α-helical structures and a concomitant increase in β-sheet structures. The onset and midpoint temperature that were determined from this plot were 48 °C and 64 °C, respectively. Two distinct bands in the amide-III region were found to be sensitive for protein denaturation. The band at 1235 cm^{-1} shows an abrupt increase in area upon denaturation (Fig. 6C), likely reflecting an increase in β-sheet structures [19]. The band at 1315 cm^{-1} shows a decrease in area upon protein denaturation (Fig. 6D), likely due to a decrease in α-helical structures [19]. The denaturation profiles that were derived using amide-III band analysis closely matched those that were determined using the amide-I or -II region. The various amide

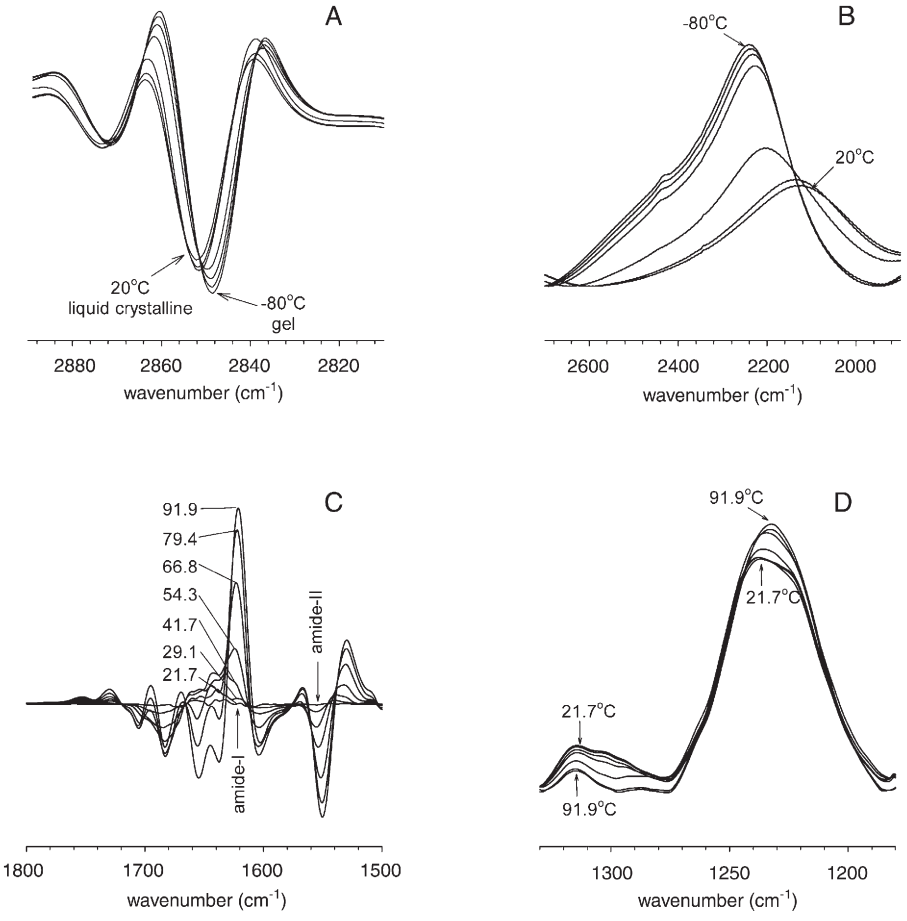

Fig. 3. Thermal FTIR analysis of LNCap cells. (A) Second derivative spectra in the lipid region show a decrease in wavenumber of the symmetric CH_2 stretching band during cooling (nucleated at −3 °C). Spectra are shown between 20 and −80 °C at increments of 16 °C. (B) The librational and bending combination mode of H_2O shows a shape change during cooling upon transition of water into ice. Spectra are shown between 20 and −80 °C at increments of 16 °C. (C) Protein denaturation at various temperatures, showing difference spectra in the amide I and II region. Each trace shown represents the spectrum obtained at a given temperature after the 20 °C spectrum was subtracted from it. (D) Shape changes in the amide-III region during heating associated with protein denaturation. The temperatures of the spectra in panel D correspond to those in panel C (increment 12 °C).

band areas were also monitored during cooling the sample back from 90 °C to 20 °C to verify that protein denaturation is irreversible. As expected, the changes in band area that were observed during heating did not reverse during cooling (data not shown).

Amide-III band analysis was also used to detect protein structural changes during freezing and thawing of the cells. Fig. 7 shows the area of the band at 1235 cm^{-1} during freezing down to −80 °C and subsequent thawing of the cells using a nucleation temperature of −3 °C. The decrease in amide-III band area coincided with the formation of ice in the system. The thawing profile closely matched the freezing profile, indicating that the freezing-induced changes in amide-III band area were reversible. The heat denaturation profile of cells that were subjected to a freeze–thaw cycle was found to be very similar to that of non-frozen control cells (Fig. 6), indicating that the freeze–thaw cycle did not affect the cells' heat denaturation characteristics. Studies at other nucleation temperatures yielded similar results.

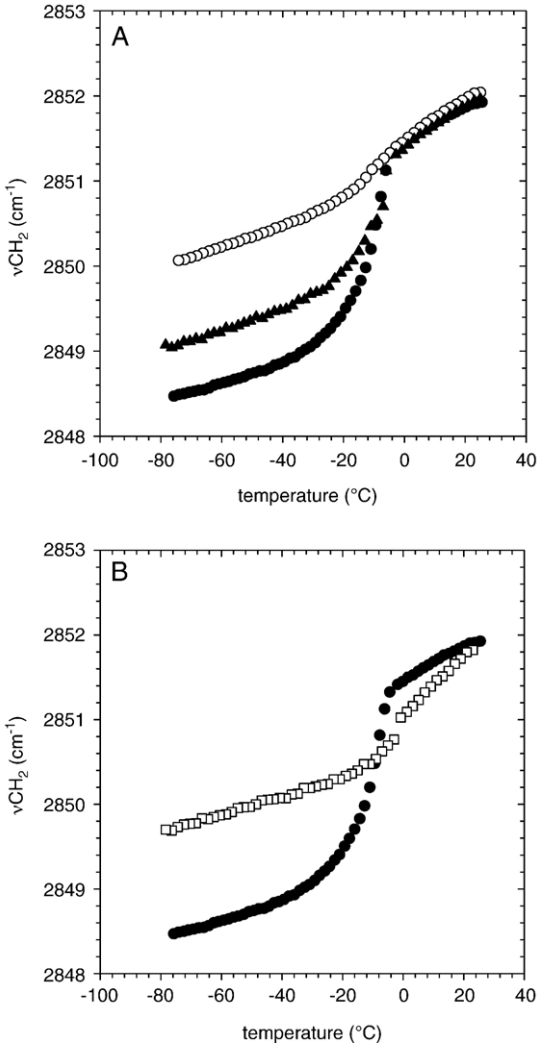

Fig. 4. Membrane phase behavior of LNCaP cells during cooling and nucleation at various subzero temperatures. (A) νCH2 versus temperature plot of during freezing the cells down to −80 °C. Samples were nucleated at −3 °C (filled circles), −6 °C (filled triangles) or at −10 °C (open circles). (B) Membrane phase behavior of cells during cooling and nucleation at −3 °C. The data points reflect those of viable control cells (filled circles) and lysed cells (open squares).

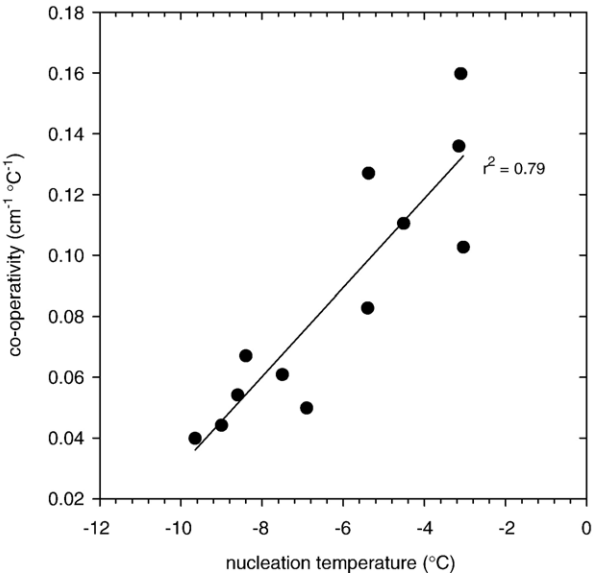

Fig. 5. Correlation between the co-operativity of the membrane phase transition of LNCaP cellular membranes during cooling and the ice nucleation temperature.

4. Discussion

FTIR was used to monitor membrane phase behavior and changes in overall protein secondary structure in LNCaP prostate tumor cells during cooling at 2 °C/min while varying the ice nucleation temperature between −3 and −10 °C. The predicted incidence of intracellular ice formation rapidly increases at ice nucleation temperatures below −4 °C and cell survival exhibits an optimum at intermediate levels of dehydration and intracellular ice formation. The ice nucleation temperature was found to have a great effect on the membrane lipid phase behavior of the cells. The onset of the liquid crystalline to gel phase transition coincides with the ice nucleation temperature. In addition, the ice nucleation temperature determines the co-operativity of the transition and the residual conformational disorder of the membranes in the frozen state. Proteins are relatively stable during freezing. Heat-induced protein denaturation is visible as an abrupt decrease in α-helical structures and a concomitant increase in β-sheet structures in good agreement with previous results [12].

Intracellular ice formation is regarded to be the main cause of injury at low nucleation temperatures or high cooling rates for different cell types [3]. Exposure to high solute concentrations (dehydration effect) is the other main cause of cell death during freezing [30]. Cells typically show optimal freezing survival at intermediate levels of dehydration and intracellular ice formation [3], which was also observed here. The effect of the nucleation temperature on the rate of intracellular ice formation has been quantified for various cell types [7,8]. These studies have established that the lower the nucleation temperature, the

greater is the incidence of intracellular ice formation in cells. The effect of the nucleation temperature on intracellular ice formation could explain the observed effects on the membrane phase behavior of the cells. LNCaP cell membranes exhibit a liquid-crystalline to gel phase transition during cooling. The membrane phase behavior, however, is strongly affected by the temperature at which ice is formed in the system. The effect of the nucleation temperature on the thermotropic response of the membranes can likely be attributed to differences in the extent of cellular dehydration. Dehydration during air-drying or freeze-drying is known to affect lipid phase behavior of liposomes and biological membranes [31–34]. Removal of water from the phospholipid head groups causes lyotropic phase transitions. Relatively few studies have been done on the effects of freezing on lipid phase behavior. A study on the effects of ice on the lipid phase behavior of pure phosphatidylethanolamine revealed that the presence of ice affected the onset temperature of the main phase transition but had little effect on the co-operativity of the transition [35]. These effects were attributed to osmotic dehydration. Interestingly, in LNCaP cells the nucleation temperature not only affected the onset temperature of the membrane phase transition but also the co-operativity and membrane fluidity in the frozen state, which we suggest is due to the extent of cellular dehydration. When nucleation is

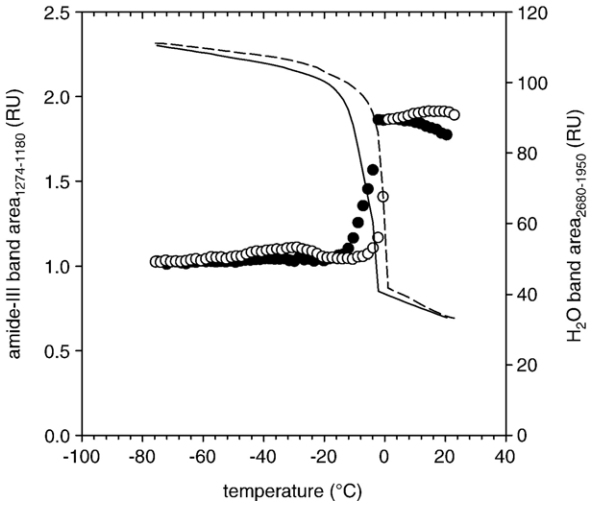

Fig. 7. Area changes in the amide-III region during freezing and thawing of LNCaP cells nucleated at −3 °C. The data points reflect the area of the band at ~1235 cm^{-1} during freezing (closed circles) and re-warming (open circles). The area of the H_2O libration and bending combination band is also shown during freezing (solid line) and thawing (dashed line) is also shown to indicate ice nucleation and ice melting.

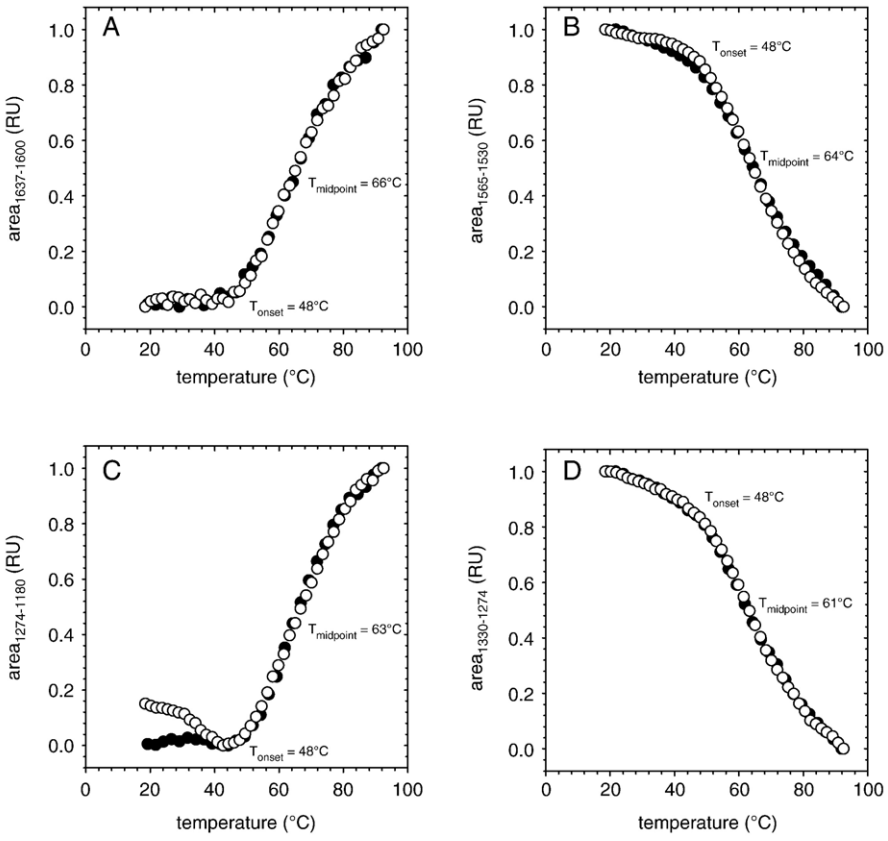

Fig. 6. Heat induced protein denaturation in LNCaP cells using amide-I, II and III band analysis. Characteristic band areas were calculated and plotted as a function of temperature. (A) Area of the band at ~1625 cm^{-1} in the amide-I region (β-sheet structures). (B) Area of the band at ~1550 cm^{-1} in the amide-II region (α-helical + β-sheet structures). (C) Area of the band at ~1235 cm^{-1} in the amide-III region (β-sheet structures). (D) Area of the band at ~1315 cm^{-1} in the amide-III region (α-helical structures). The data points reflect band areas during heating of non frozen control cells (closed circles), and cells that were subjected to a freeze–thaw cycle to −80 °C (open circles).

initiated between 0 and −4 °C, intracellular ice formation is avoided and the cells will start to dehydrate upon ice formation in the extracellular space. Dehydration is manifested as a decrease in membrane fluidity in the frozen state due to a decrease in hydration level of the water around the phospholipid head groups. When ice nucleation occurs below −4 °C, the incidence of intracellular ice formation increases, resulting in a greater residual conformational disorder of the cell membranes in the frozen state, indicating that membranes remain relatively hydrated under those conditions. Lysed cells that are nucleated at temperatures where intracellular ice formation is avoided in intact cells show membrane phase behavior indicative of intracellular ice formation. This is likely due to a loss of membrane integrity upon lysis of the cells, which increases the incidence of intracellular ice formation.

Denaturation of proteins can be brought about by both heat and cold. Heat denaturation of many proteins typically occurs at measurable rates above 50 °C [36]. On the other hand, cold denaturation typically occurs in the range of 0 to 20 °C [37,38], although this was not observed in this study.

We previously showed that heat-induced protein denaturation in cells can be measured *in situ* using changes in the amide-I band profile [12]. This approach yields denaturation profiles that closely resemble those determined by DSC [39]. The denaturation profile is cell or tissue specific and can be used as a thermal fingerprint. We show here that the amide-III region can also be used to detect protein denaturation in cells. The amide-III region has the advantage that the different types of secondary structure are better resolved and that water bands do not interfere [19,40]. The shape changes in amide-III band profile that were observed during heat denaturation of LNCaP cells have also been observed during denaturation of isolated proteins [40]. It should be noted that the amide-III region of cells may also contain contributions from other molecular group vibrations, particularly the asymmetric phosphate stretching vibration. Nevertheless, the denaturation profiles that were derived using amide-III band analysis closely matched those that were determined using amide-I or -II band analysis, which indicates that the thermotropic response of the bands in the amide-III region for the most part can be assigned to protein denaturation. The observed reduction in α-helical structures and concomitant increase in β-sheet structures is typically observed during heat denaturation of proteins [12,18,23,41]. The overall protein secondary structure of LNCaP cells was found to be relatively stable during freezing. During cooling, a decrease in amide-III band area was observed at the ice nucleation temperature, likely because the amide vibrational modes form different hydrogen bonds with water upon ice formation in the system. The effect of ice nucleation on the amide-III band area was found to be reversible. The heat denaturation profile of frozen cells closely resembled that of non-frozen control cells, suggesting that freezing only had minor effects on the overall protein secondary structure. In AT-1 Dunning cells, freezing to −80 °C partially denatured cellular proteins which affected the heat denaturation profile [12]. The freezing and thawing conditions, however, were different from the conditions that were used here.

Acknowledgement

This project was financially supported by the National Institute of Health (NIH) R01-CA07528.

References

[1] P.R. Stauffer, S.N. Goldberg, Introduction: thermal ablation therapy, Int. J. Hyperthermia 20 (2004) 671–677.
[2] A. Porter, P. Littrup, D. Grignon, J. Forman, J. Montie, Radiotherapy and cryotherapy for prostate cancer, in: P. Walsh, A. Retik, E. Vaughan, A. Wein (Eds.), Campbell's Urology, Saunders Co, Philadelphia, 1998, pp. 2605–2626.
[3] P. Mazur, S.P. Leibo, E.H. Chu, A two-factor hypothesis of freezing injury. Evidence from Chinese hamster tissue-culture cells, Exp. Cell Res. 71 (1972) 345–355.
[4] P. Mazur, Principles of cryobiology, in: B.J. Fuller, E.E. N.Lane (Eds.), Life in the Frozen State, CRC Press, Boca Raton, FL, 2004, pp. 3–65.
[5] P. Mazur, K.W. Cole, Roles of unfrozen fraction, salt concentration, and changes in cell volume in the survival of frozen human erythrocytes, Cryobiology 26 (1989) 1–29.
[6] P. Mazur, S. Seki, I.L. Pinn, F.W. Kleinhans, K. Edashige, Extra- and intracellular ice formation in mouse oocytes, Cryobiology 51 (2005) 29–53.
[7] R.E. Pitt, M. Chandrasekaran, J.E. Parks, Performance of a kinetic model for intracellular ice formation based on the extent of supercooling, Cryobiology 29 (1992) 359–373.
[8] J.O. Karlsson, E.G. Cravalho, I.H. Borel Rinkes, R.G. Tompkins, M.L. Yarmush, M. Toner, Nucleation and growth of ice crystals inside cultured hepatocytes during freezing in the presence of dimethyl sulfoxide, Biophys. J. 65 (1993) 2524–2536.
[9] M. Caffrey, The combined and separate effects of low temperature and freezing on membrane lipid mesomorphic phase behavior: Relevance to cryobiology, Biochim. Biophys. Acta 896 (1987) 123–127.
[10] J.H. Crowe, L.M. Crowe, D. Chapman, Preservation of membranes in anhydrobiotic organisms: the role of trehalose, Science 223 (1984) 701–703.
[11] J.F. Brouwers, B.M. Gadella, In situ detection and localization of lipid peroxidation in individual bovine sperm cells, Free Radical Biol. Med. 35 (2003) 1382–1391.
[12] J.C. Bischof, W.F. Wolkers, N.M. Tsvetkova, A.E. Oliver, J.H. Crowe, Lipid and protein changes due to freezing in Dunning AT-1 cells, Cryobiology 45 (2002) 22–32.
[13] B.S. Berlett, E.R. Stadtman, Protein oxidation in aging, disease, and oxidative stress, J. Biol. Chem. 272 (1997) 20313–20316.
[14] D.G. Cameron, A. Martin, H.H. Mantsch, Membrane isolation alters the gel to liquid crystal transition of *Acholeplasma laidlawii* B, Science 219 (1983) 180–182.
[15] J. Bandekar, Amide modes and protein conformation, Biochim. Biophys. Acta 1120 (1992) 123–143.
[16] W.K. Surewicz, H.H. Mantsch, D. Chapman, Determination of protein secondary structure by Fourier transform infrared spectroscopy: a critical assessment, Biochemistry 32 (1993) 389–394.
[17] E. Goormaghtigh, V. Cabiaux, J.M. Ruysschaert, Determination of soluble and membrane protein structure by Fourier transform infrared spectroscopy: I. Assignments and model compounds, Sub-cell. Biochem. 23 (1994) 329–362.
[18] W.F. Wolkers, F.A. Hoekstra, In situ FTIR assessment of desiccation-tolerant tissues, Spectroscopy 17 (2003) 297–313.
[19] S. Cai, B.R. Singh, A distinct utility of the amide III infrared band for secondary structure estimation of aqueous protein solutions using partial least squares methods, Biochemistry 43 (2004) 2541–2549.
[20] M. van de Weert, P.I. Haris, W.E. Hennink, D.J.A. Crommelin, Fourier transform infrared spectrometric analysis of protein conformation: effect of sampling method and stress factors, Anal. Biochem. 297 (2001) 160–169.
[21] R.V. Devireddy, D.J. Swanlund, A.S. Alghamdi, L.A. Duoos, M.H.T. Troedsson, J.C. Bischof, K.P. Roberts, Measured effect of collection and

cooling conditions on the motility and the water transport parameters at subzero temperatures of equine spermatozoa, Reproduction 124 (2002) 643–648.
[22] W.F. Wolkers, L.M. Crowe, N.M. Tsvetkova, F. Tablin, J.H. Crowe, In situ assessment of erythrocyte membrane properties during cold storage, Mol. Membr. Biol. 19 (2002) 59–65.
[23] W.F. Wolkers, F.A. Hoekstra, Heat stability of proteins in desiccation-tolerant cattail (*Typha latifolia* L.) pollen: a Fourier transform infrared spectroscopic study, Comp. Biochem. Physiol. 117 (1997) 349–355.
[24] P. Mazur, Kinetics of water loss from cells at subzero temperatures and the likelihood of intracellular freezing, J. Gen. Physiol. 47 (1963) 347–369.
[25] R.L. Levin, E.G. Cravalho, C.E. Huggins, Effect of hydration on the water content of human erythrocytes, Biophys. J. 16 (1976) 1411–1426.
[26] M. Toner, E.G. Cravalho, M. Karel, Thermodynamics and kinetics of intracellular ice formation during freezing of biological cells, J. Appl. Phys. 67 (1990) 1582–1593.
[27] M.S. Berrada, J.C. Bischof, Evaluation of freezing effects on human microsvascular endothelial cells (hMEC), Cryo-Letters 22 (2001) 353–366.
[28] D.J. Smith, M. Schulte, J.C. Bischof, The effect of dimethylsulfoxide on the water transport response of rat hepatocytes during freezing, J. Biomech. Eng. 120 (1998) 549–558.
[29] S.K. Balasubramanian, J.C. Bischof, A. Hubel, Water transport and IIF parameters for a connective tissue equivalent, Cryobiology 52 (2006) 62–73.
[30] J.E. Lovelock, The haemolysis of human red blood-cells by freezing and thawing, Biochim. Biophys. Acta 10 (1953) 414–426.
[31] J.H. Crowe, F.A. Hoekstra, L.M. Crowe, T.J. Anchordoguy, E. Drobnis, Lipid phase transitions measured in intact cells with Fourier transform infrared spectroscopy, Cryobiology 26 (1989) 76–84.
[32] J.H. Crowe, A.E. Oliver, F.A. Hoekstra, L.M. Crowe, Stabilization of dry membranes by mixtures of hydroxyethyl starch and glucose: the role of vitrification, Cryobiology 35 (1997) 20–30.
[33] A.V. Popova, D.K. Hincha, Effects of the sugar headgroup of a glycoglycerolipid on the phase behavior of phospholipid model membranes in the dry state, Glycobiology 15 (2005) 1150–1155.
[34] H. Oldenhof, W.F. Wolkers, J.L. Bowman, F. Tablin, J.H. Crowe, Freezing and desiccation tolerance in the moss *Physcomitrella patens*: an in situ Fourier transform infrared spectroscopic study, Biochim. Biophys. Acta 1760 (2006) 1226–1234.
[35] P.W. Sanderson, W.P. Williams, B.A. Cunningham, D.H. Wolfe, L.J. Lis, The effect of ice on membrane lipid phase behaviour, Biochim. Biophys. Acta 1148 (1993) 278–284.
[36] H. Eyring, Temperature, in: F.H. Johnson, H. Eyring, B.J. Stover (Eds.), The Theory of Rate Processes in Biology and Medicine, John Wiley and Sons, New York, 1974, pp. 155–272.
[37] P.L. Privalov, Cold denaturation of proteins, Crit. Rev. Biochem. Mol. Biol. 25 (1990) 281–305.
[38] X. Tang, M.J. Pikal, The effect of stabilizers and denaturants on the cold denaturation temperatures of proteins and implications for freeze-drying, Pharm. Res. 22 (2005) 1167–1175.
[39] X. He, W.F. Wolkers, J.H. Crowe, D.J. Swanlund, J.C. Bischof, In situ thermal denaturation of proteins in Dunning AT-1 prostate cancer cells: implication for hyperthermic cell injury, Ann. Biomed. Eng. 32 (2004) 1384–1398.
[40] G. Anderle, R. Mendelsohn, Thermal denaturation of globular proteins. Fourier transform-infrared studies of the amide III spectral region, Biophys. J. 52 (1987) 69–74.
[41] W.F. Wolkers, M. Alberda, M. Koornneef, K.M. Léon-Kloosterziel, F.A. Hoekstra, Properties of proteins and the glassy matrix in maturation-defective mutant seeds of *Arabidopsis thaliana*, Plant J. 16 (1998) 133–143.